A deep learning approach for anomaly identification in PZT sensors using point contact method

OPEN ACCESS
IOP Publishing
Smart Materials and Structures
Smart Mater. Struct. **32** (2023) 095027 (14pp)
https://doi.org/10.1088/1361-665X/acee37

A deep learning approach for anomaly identification in PZT sensors using point contact method

Nur M M Kalimullah[1], **Amit Shelke**[1] and **Anowarul Habib**[2,*]

[1] Department of Civil Engineering, Indian Institute of Technology Guwahati, Guwahati, Assam, 781039, India
[2] Department of Physics and Technology, UiT The Arctic University of Norway, 9037 Tromsø, Norway

E-mail: anowarul.habib@uit.no

Received 23 May 2023, revised 25 July 2023
Accepted for publication 8 August 2023
Published 21 August 2023

Abstract

The implementation of piezoelectric sensors is degraded due to surface defects, delamination, and extreme weathering conditions, to mention a few. Hence, the sensor needs to be diagnosed before the efficacious implementation in the structural health monitoring (SHM) framework. To rescue the problem, a novel experimental method based on Coulomb coupling is utilised to visualise the evolution of elastic waves and interaction with the surface anomaly in the lead zirconate titanate (PZT) substrate. Recently, machine learning (ML) has been expeditiously becoming an essential technology for scientific computing, with several possibilities to advance the field of SHM. This study employs a deep learning-based autoencoder neural network in conjunction with image registration and peak signal-to-noise ratio (PSNR) to diagnose the surface anomaly in the PZT substrate. The autoencoder extracts the significant damage-sensitive features from the complex waveform big data. Further, it provides a nonlinear input–output model that is well suited for the non-linear interaction of the wave with the surface anomaly and boundary of the substrate. The measured time-series waveform data is provided as input into the autoencoder network. The mean absolute error (MAE) between the input and output of the deep learning model is evaluated to detect the anomaly. The MAEs are sensitive to the anomaly that lies in the PZT substrate. Further, the challenge arising from offset and distortion is addressed with ad hoc image registration technique. Finally, the localisation and quantification of the anomaly are performed by computing PSNR values. This work proposes an advanced, efficient damage detection algorithm in the scenario of big data that is ubiquitous in SHM.

Keywords: anomaly detection, autoencoder, Coulomb coupling, neural network, PZT, SHM

(Some figures may appear in colour only in the online journal)

1. Introduction

Recently, lead zirconate titanate ($PbZr_xTi_{1-x}O_3$) is commonly recognised as PZT and has developed as an excellent choice to generate ultrasonic waves for various engineering and scientific applications. The remarkable features of PZT are less energy consumption, negligible mass, economical, ease of use in the field application, wideband frequency response and physical robustness, to mention a few. The PZT substrates play a critical role in various military and engineering applications. For instance, these materials are employed in telecommunication, optoelectronics, actuators, biomedical equipment, energy harvesting devices and structural health monitoring (SHM) [1–5]. SHM has emerged on diagnosis, etiognosis and prognosis to reduce the life cycle costs of civil

* Author to whom any correspondence should be addressed.

and mechanical structures [6, 7]. In the SHM, PZT transducers are often employed in active and passive modes for damage detection of the structure and further localising the damage at the microscale [8]. However, the reliability and precision of assessing such structures substantially depend on the quality of the PZT sensors. Under the rigorous functional environment, the sensor's health may decline due to fatigue, exposure to humidity, extreme temperature fluctuation, and corrosion, to mention a few. These harsh conditions are likely to be developed micro-defects within the sensor. Therefore, it is imperative to identify and localise the anomaly of PZT sensors arising from surface defect, corrosion and delamination in order to avoid the SHM false alarm and shutting down the monitoring process [9–11]. Coming to the rescue, the current research presents a novel framework based on a deep autoencoder neural network (NN) to identify the anomaly in the PZT sensor.

Over the years, several non-destructive evaluation (NDE) and SHM methods have evolved and been implemented for the detection of failure in important structures [12, 13]. Various non-destructive methodologies, including nano-indentation, Raman spectroscopy, and neutron diffraction, are utilised to characterise the PZT films [13, 14]. However, these techniques give localised information on the mechanical properties of the materials. Further, active sensing based on lamb and surface acoustic waves enhances damage detection and material characterisation. These methods are sensitive to the damage but less captivating in subsurface aberration [15–18].

In recent years, our group has optimised the point contact excitation and detection method to visualise the evolution of ultrasonic waves in piezoelectric materials [19–22]. This novel experimental technique is manifested to excite and detect bulk and guided waves, the metamorphosis of lamb and surface waves by exciting phonon vibration in piezoelectric substrates [19–23]. The governing principle of the excitation of phonon vibration is the transformation of the electric field into mechanical energy in the piezoelectric material [24]. The comprehensive working principle and advantages over different NDE techniques are found in the literature and omitted herein [20, 23].

A probe made of a gold or steel sphere acts as a Coulomb electrode to excite and detect ultrasonic waves. The influence of probe radius on ultrasonic wave propagation is illustrated by Habib *et al* [25]. This work augments the point contact method to visualise the interaction of the spatial–temporal evolution of waves with the surface anomaly in the sintered piezoelectric substrate. The wave suffers from multiple reflections and interferences with the backward propagating wave when the forward propagating wave encounters the surface defect and boundaries of the material. These interactions with edges and defects often lead to a mode conversion resulting in spatial and temporal dispersion. In such a scenario, localising and quantifying the defect from the wave visualisation is challenging. Thus, it is crucial to extract the damage-sensitive features from the big data collected by performing the experiment.

The temporal signal received by the ultrasonic wave excitation is often considered in the SHM framework for condition monitoring [19, 23]. The diagnosis of a structural system using ultrasonic-based methods can be reformed as a pattern recognition problem that constitutes three essential steps: (a) feature extraction, (b) feature selection, and (c) damage classification. Recently, the artificial NN (ANN) and support vector machine (SVM) are the widely used pattern recognition algorithm for the diagnosis of structural and mechanical systems [26–28]. However, these methods have three inherent shortcomings. To begin with, the received signals are often non-linear and non-stationary, and the significant damage-sensitive features are overwhelmed by the background noise [29]. Hence, advanced signal processing techniques need to be adopted for effective feature extraction. In addition, hand-designed features are selected based on the specific fault diagnosis scenario; however, the features are generally not portable for a new scenario [30]. Finally, perhaps most importantly, these are shallow architectures with no more than one non-linear transformation [31]. Several studies have illustrated that shallow architectures perform inadequately in representation and learning complex non-linear relationship that is ubiquitous for the current damage diagnosis scenario [32, 33]. Thus, it is imperative to create a deep framework for anomaly identification.

NNs, which construct the underlying architecture of deep learning, are widely employed across the various science and engineering domains [34–37]. The first NN architecture was named Neocognitron, which shares many characteristic features with modern deep NNs containing multi-layer structure, max pooling, convolution, and non-linear dynamical nodes, to mention a few [38]. Notably, the universal approximation theorem promises that a NN comprised of enough hidden units and linear output is competent in depicting any arbitrary function or dataset, including our complex waveform data [39–41]. Indeed, deep learning succeeds in transformative development in several data-driven classification and regression tasks [42, 43]. An advantage of deep learning is that it can represent a complex function by extracting the features of the data hierarchically. Thus, deep learning can correctly approximate a function without manually choosing features or informing the user-defined basis [43].

Deep learning has gained lots of traction across scientific computing and offers several possibilities to advance the domain of SHM. The methods based on deep learning framework are extensively employed to diagnose the civil and mechanical structures and have shown promising results [44–47]. The ANN and other deep-learning frameworks are used to detect anomalies in composite structures by utilising vibration and frequency-based approaches [48, 49]. Several researchers have utilised guided waves in conjunction with the deep-learning architecture to detect damage in composite structures [50–52]. Further, Melville *et al* utilised classical machine learning (ML) methods, SVM and deep-learning algorithms for detecting anomaly in the full wavefield images [53]. The wavefield images are collected by employing the piezoelectric actuators and laser Doppler vibrometer. It is reported that the

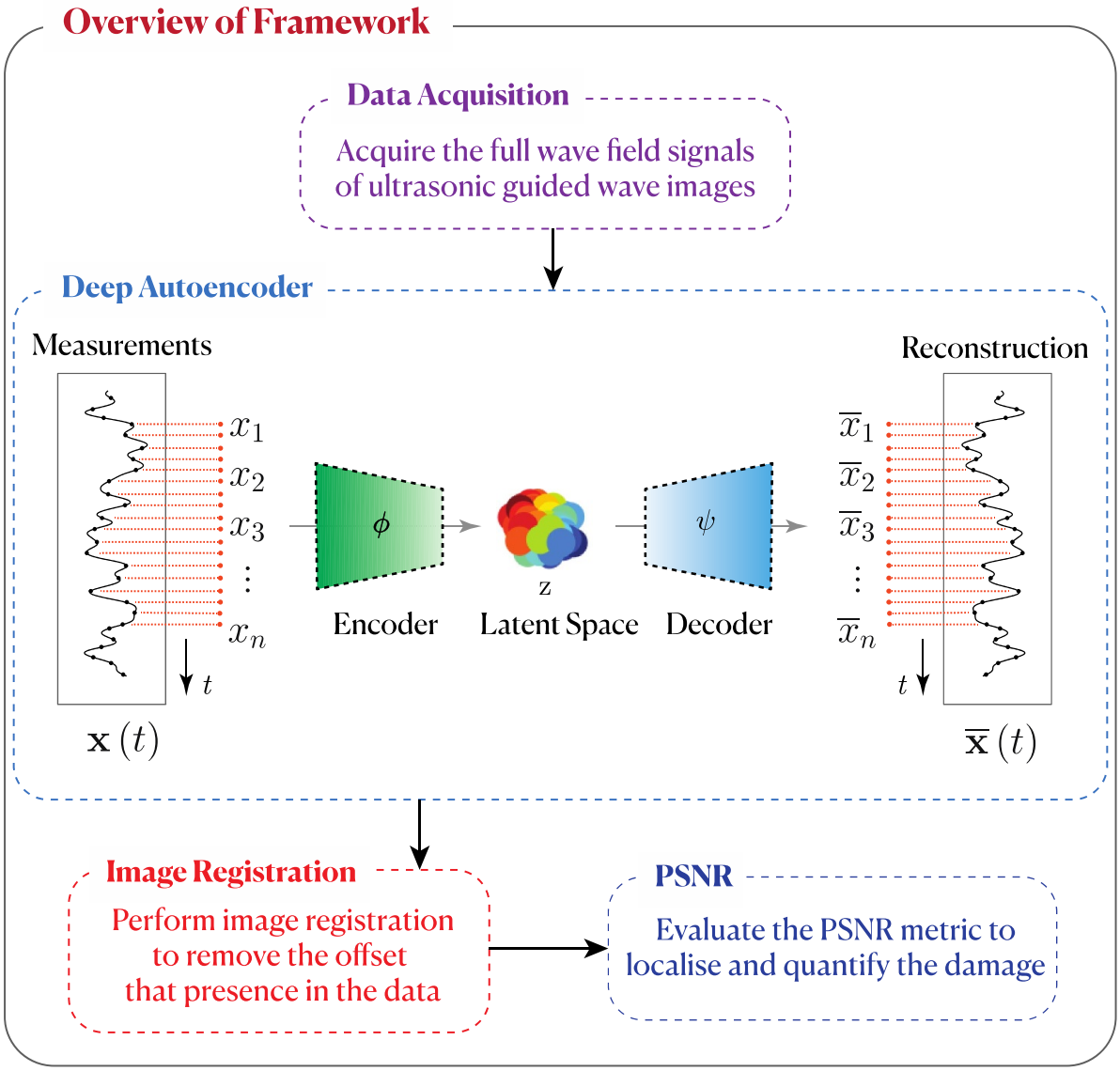

Figure 1. The overview of the proposed damage detection algorithm.

deep learning methods achieve better performance in damage detection as compared to the SVM-based methods.

This work presents a novel damage detection framework based on a deep autoencoder NN, image registration [54] and peak signal-to-noise ratio (PSNR) [55]. The proposed method is applied for the diagnosis of PZT substrate using propagation of the ultrasonic wave. The results show that the proposed method is robust, reliable and effective for the SHM framework. The advantages of the building block used in the proposed frameworks are as follows:

- In order to avoid conventional signal processing techniques and diagnose experience, a damage detection framework is proposed primarily based on the deep autoencoder feature learning method to learn the necessary damage-sensitive features from the experimental measurement automatically.
- In order to nullify the error due to the offset presented in the experimental data and to enhance the performance, the image registration technique is employed.
- In order to localisation and quantify the damage, the PSNR metric is adopted.

The overview of the proposed framework is illustrated in figure 1. The rest of the paper is organised as follows. In section 2, we first provide an overview of the experimental setup and discuss the data acquisition process by performing an experiment. Section 3 presents the mathematical background of a deep autoencoder network. The image registration process and PSNR technique are discussed in sections 4 and 5, respectively. In section 6, the results are provided to illustrate the efficacy of the proposed framework. The paper ends with some conclusions in section 7.

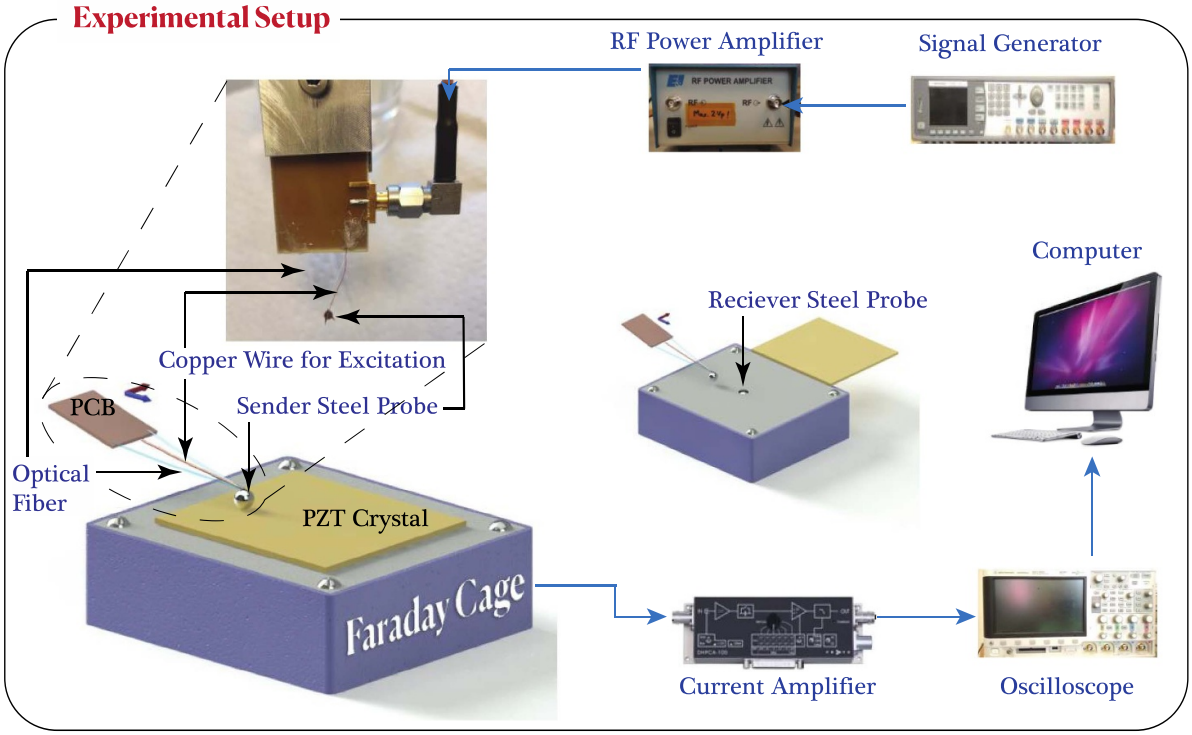

Figure 2. Experimental setup for point contact excitation and detection method.

2. Experimental setup

A comprehensive report of the experimental setup, excitation and detection principles, and probe fabrication is outlined in the literature by our group [19–22]. This state-of-the-art experimental technique based on Coulomb coupling is developed for the excitation and detection of ultrasonic waves in a piezoceramic [56]. The electric field gradient and piezoelectric properties gradient control the transformation of electromagnetic energy to acoustic energy via Coulomb coupling in a piezoelectric material. A Coulomb coupling technique is based on generating the electric field that induces stress waves by electro-mechanical excitation [57]. The experimental technique is tuned for effective electric field coupling with elastic modulus and permittivity of piezoceramics. Figure 2 illustrates the experimental setup for point contact excitation and detection in PZT ceramic samples.

An arbitrary function generator (Agilent 81150A) generated the excitation Dirac delta pulse of 70 ns time width. The generated signal was delivered to a radio-frequency amplifier (Electronics and Innovation: 403LA, New York, USA) for signal amplification. These amplified signals were then routed to the excitation steel probe. The steel sphere made gentle contact with the surface of the PZT sample. The excited signal induced acoustic waves in the specimen. On the opposite surface of the PZT, a similar steel probe was employed for the acquisition of the acoustic waves. The acquired waves were then amplified by a trans-impedance amplifier (DHPCA-100). This type of amplifier can transform current into voltage with an adjustable amplification factor. Lastly, the amplified signal was acquired by an oscilloscope (Agilent 3024A) capable of digitising up to 12 bits. The sampling interval of data collection was 25 ns. The oscilloscope conducts averaging of 256 pulse shootings and digitises the signal, which is then stored in a personal computer (PC) via a USB port. The PC was also employed to control the mechanical scanner in the *XY* plane. The scanning area was 10 mm × 10 mm, with the step size being 50 μm in both directions.

The goal of performing the experiment is to visualise the spatial–temporal evolution of ultrasonic waves in the PZT sample to identify the anomaly. Towards that, a healthy specimen of PZT is placed in the setup, and the Coulomb scanning is performed. After the scanning, controlled surface damage is introduced by a diamond drill. The dimension of the damage is about 1.2 mm × 1.3 mm and depth of 1.5 mm. Figure 3 demonstrates the image of the surface anomaly. The interaction of the wave with the anomaly is visualised by scanning the damaged specimen again.

Closing this section, it is worth mentioning that the limit of the point contact excitation and detection method primarily depends upon few parameters, that is, the diameter of the probe, time gating of the excitation pulse, to mention a few. The obtainable resolution of the Coulomb excitation method as mentioned in the study carried by Habib *et al* is $\lambda/2$, where λ is the acoustic wavelength [25]. Further, it is mentioned that to obtain a resolution equivalent to Abbe limit, the approximate diameter of the probe is given as $D = \lambda/0.24$. In the current setting, the resolution equivalent to the diffraction limit is computed approximately as 308 μm.

Figure 3. Image of the surface anomaly in PZT substrate having a dimension of 1.2 mm × 1.3 mm and 1.5 mm in depth.

3. Mathematical background of deep autoencoder

To discuss the mathematical background of deep autoencoder, let us first discuss the construction spatiotemporal data matrix, $\mathcal{D}$. The time domain signals are recorded by employing point contact excitation and detection method by placing the sender probe at p points along the x-direction and q points along y-directions, which is the total $(p \times q)$ number of spatial points on the substrate. By stacking all the $(p \times q)$ number of signals, the data matrix $\mathcal{D}$ is constructed given in equation (1)

$$\mathcal{D} = \{\mathbf{S}_1, \mathbf{S}_2, \mathbf{S}_3, \ldots, \mathbf{S}_m\}_{(p\times q\times m)}. \tag{1}$$

One can create a two-dimensional (2D) matrix by collecting the measurement at the ith index $(1 \leqslant i \leqslant m)$ of the time domain signal. This matrix represents the 2D snapshots of the wavefield denoted by $\mathbf{S}_i$ in equation (1). $\mathcal{D}$ represents the collection of the 2D snapshot of wavefield images. The dimension of each snapshot is $p \times q$, where p, q represent the number of pixels along x- and y-directions, respectively. There exist m such snapshots along the time axis. It is possible to vectorise each snapshot matrix, $\mathbf{S}_i$ to a higher dimensional, for instance, n-dimensional $(n = p \times q \geqslant 1)$ column vector, $\mathbf{x}_i$. Each column of the matrix $\mathbf{X}$ represents the vectorised form of each snapshot as given in equation (2)

$$\mathbf{X} = \{\mathbf{x}_1, \mathbf{x}_2, \ldots, \mathbf{x}_m\}_{n\times m}. \tag{2}$$

A deep autoencoder NN is an amenable and expedient framework for exploiting low-dimensional meaningful features from high-dimensional data. The autoencoder generalises the linear subspace embedding of singular value decomposition or principal component analysis to a nonlinear manifold embedding, often of a lower dimension [58, 59]. Specifically, for the given training data $\mathbf{X} = \{\mathbf{x}_1, \mathbf{x}_2, \ldots, \mathbf{x}_m\}$ (for each sample $\mathbf{x}_i$, $\mathbf{x}_i = [x_1, x_2, \ldots, x_n]^T$), the encoder maps the original high-dimensional input vector $\mathbf{x}_i \in \mathbb{R}^n$ to a low-dimensional latent representation $\mathbf{Z} = \{\mathbf{z}_1, \mathbf{z}_2, \ldots, \mathbf{z}_m\}$ (for each $\mathbf{z}_i \in \mathbb{R}^r$, $\mathbf{z}_i = [z_1, z_2, \ldots, z_r]^T$). Then the latent representation $\mathbf{Z}$ is transformed back to the high dimensional space $\bar{\mathbf{X}} = \{\bar{\mathbf{X}}_1, \bar{\mathbf{X}}_2, \ldots, \bar{\mathbf{X}}_m\}$ (for each $\bar{\mathbf{X}}_i \in \mathbb{R}^n$, $\bar{\mathbf{X}}_i = [\bar{x}_1, \bar{x}_2, \ldots, \bar{x}_n]^T$) by the decoder, which is technically the output of the network. The objective of the autoencoder is to map the output back to itself, i.e. $\|\bar{\mathbf{x}} - \mathbf{x}\|_2 \approx 0$. Usually, $r \ll n$ for autoencoding and mathematically, the encoding is represented as

$$\mathbf{Z} = \phi(\mathbf{X}), \tag{3}$$

where $\mathbf{Z}$ is the latent space data and $\mathbf{X}$ is the training high-dimensional input data. Decoding is represented as

$$\bar{\mathbf{X}} = \psi(\mathbf{Z}), \tag{4}$$

where the NN parameters are tuned so that the output $\bar{\mathbf{X}}$ is as accurate as possible to the input $\mathbf{X}$,

$$\arg\min_{\theta} \left\|\mathbf{X} - \bar{\mathbf{X}}\right\|_2^2 = \arg\min_{\theta} \|\mathbf{X} - \mathbf{f}_\theta(\mathbf{X})\|_2^2, \tag{5}$$

where θ are the learnable parameters of the autoencoder network $\mathbf{f}_\theta(\mathbf{x}) = \psi(\phi(\mathbf{x}))$.

From a mathematical point of view, the autoencoder allows a mapping, as shown in figure 4, so that

$$\begin{aligned} \phi &: \mathcal{X} \to \mathcal{Z}, \\ \psi &: \mathcal{Z} \to \mathcal{X}, \end{aligned} \tag{6}$$

where the input $\mathbf{x} \in \mathcal{X} \subseteq \mathbb{R}^n$ and output $\mathbf{z} \in \mathcal{Z} \subseteq \mathbb{R}^r$ are defined in high- and low-dimensional spaces, respectively. The final NN optimisation is composed around the loss function as represented in equation (7)

$$\arg\min_{\phi,\psi} \|\mathbf{X} - (\psi \circ \phi)\mathbf{X}\|. \tag{7}$$

4. Image registration

Image registration is the process of aligning two or more images of the same scene or object from several perspectives or sensors [54, 60]. Generally, the sensed images are geometrically aligned with respect to the reference image. The objective of the image registration is to bring the images into a

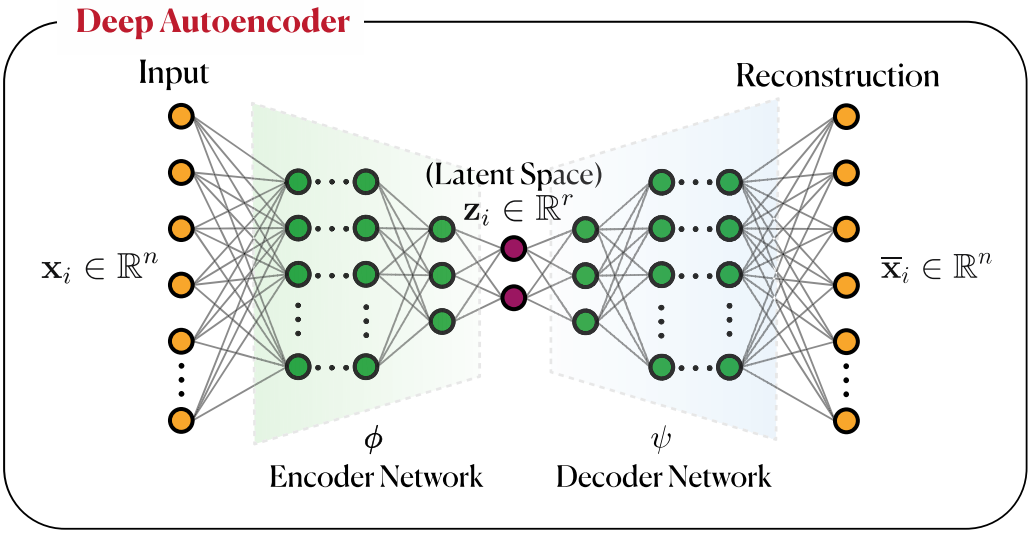

Figure 4. Illustration of an autoencoder network architecture.

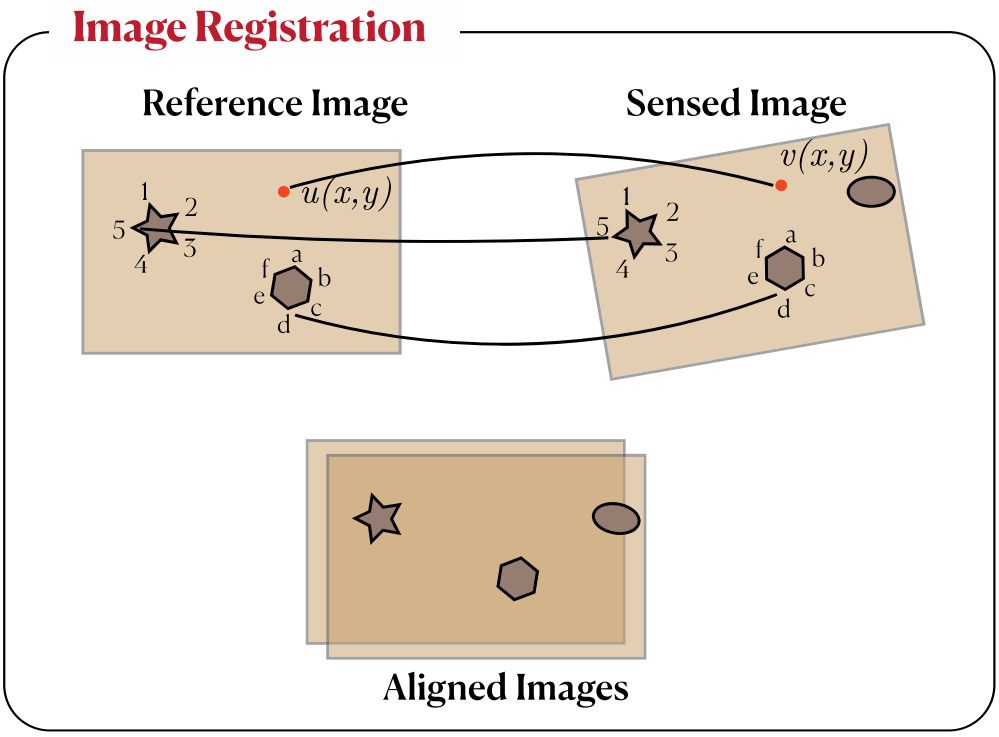

Figure 5. Illustration of the steps involved in the image registration process.

common reference frame so that they can be easily compared and fused. This method is widely employed in medical imaging, satellite imagery and computer vision.

There are several techniques that can be utilised to perform image registration, including feature-based methods, intensity-based methods, and phase-based methods. Feature-based methods comprise detecting and matching corresponding features in the images, such as points, edges or corners. Intensity-based methods involve comparing the intensity values of corresponding pixels in the images. Phased-based methods, also known as phase correlation, utilise the phase information in the image to align them. The choice of the method for image registration depends on the type of image, the amount of noise in the image and the desired accuracy in the registration. A schematic illustration showing the image registration process is presented in figure 5.

Finding the similarity is a crucial building block of the proposed damage detection algorithm. The mean absolute error (MAE) in the reconstruction from healthy data using deep autoencoder is considered a reference image, and from damaged data is considered a sensed image. After registering these images, they are compared based on the content. Here

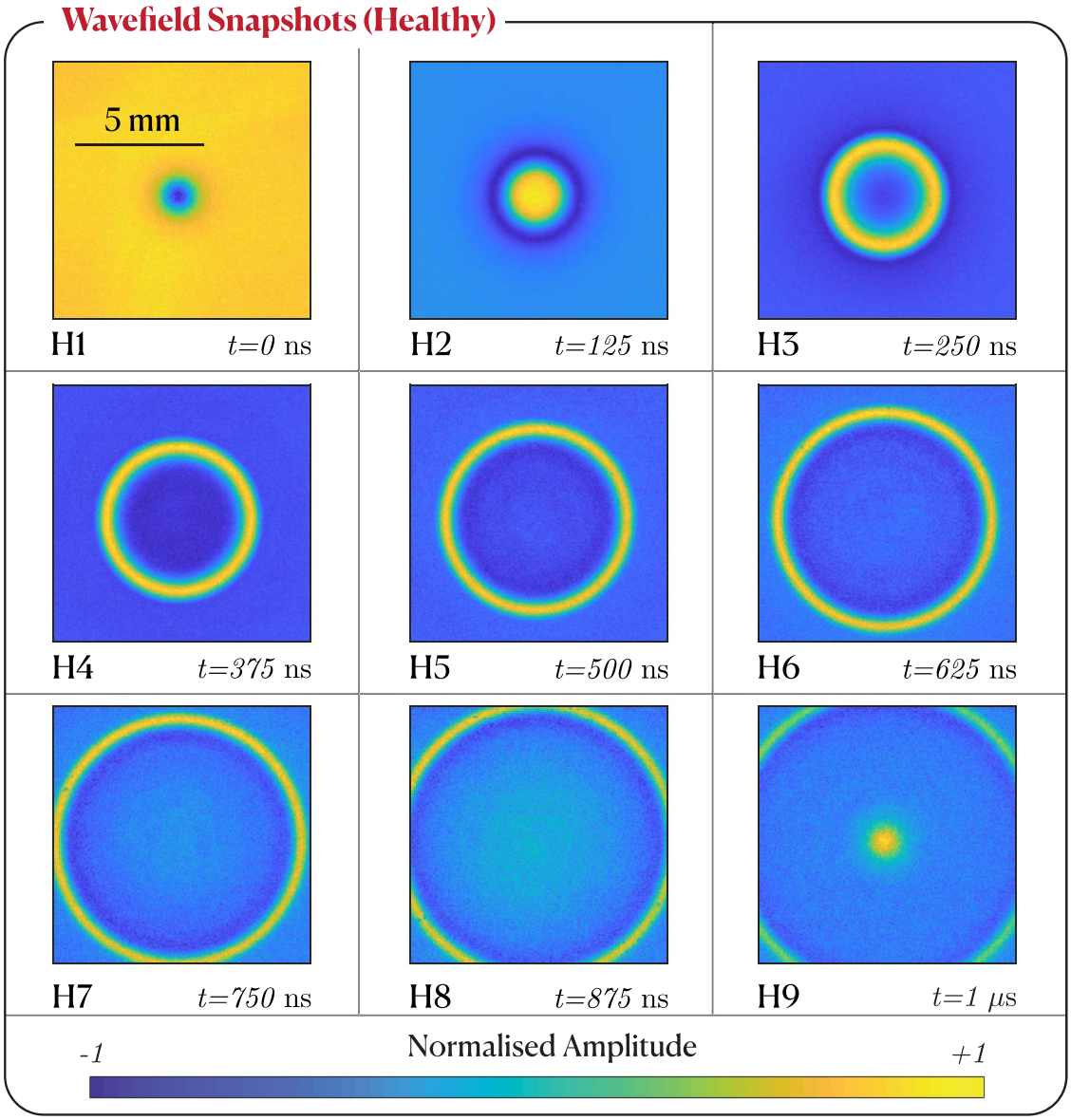

Figure 6. Sequential snapshots of the spatial and temporal evolution of the ultrasonic waves at an interval of 125 ns in a 3 mm thick sintered PZT (healthy state). The dimension of each frame is 10 mm × 10 mm.

in this work, PSNR is employed for the comparison of the images. In the following section, PSNR is briefly discussed.

5. PSNR

PSNR is a measure of the quality of reconstructed or compressed data. It is widely used to measure the image quality of image compression and image restoration system. The PSNR is usually defined via the mean squared error (MSE). It is typically expressed in decibels (dB). Given a reference image $I_1(m,n)$ and the sensed image $I_2(m,n)$ of size $M \times N$, the MSE and thus PSNR (in dB) is defined as

$$\mathrm{MSE} = \frac{1}{MN}\sum_{M,N}\left[I_1(m,n) - I_2(m,n)\right]^2, \tag{8}$$

$$\mathrm{PSNR} = 10\log_{10}\left(\frac{\mathrm{Max}_i{}^2}{\mathrm{MSE}}\right). \tag{9}$$

Here, Max_i is the maximum possible pixel value of the image. The higher the PSNR, the better the similarity between the sensed and reference images since a higher PSNR indicates a lower MSE and, thus, less distortion. Note that, PSNR $= \infty$, if $I_1(m,n) = I_2(m,n)$ (since MSE $= 0$) indicates self-identification and PSNR $< \infty$ for all $I_1(m,n)$ and $I_2(m,n)$.

6. Results and discussion

This section presents the results by implementing the proposed novel and robust anomaly detection algorithm. Figure 6 presents the visualisation 2D acoustic wave propagation in the PZT ceramic. The time interval of the snapshots shown in

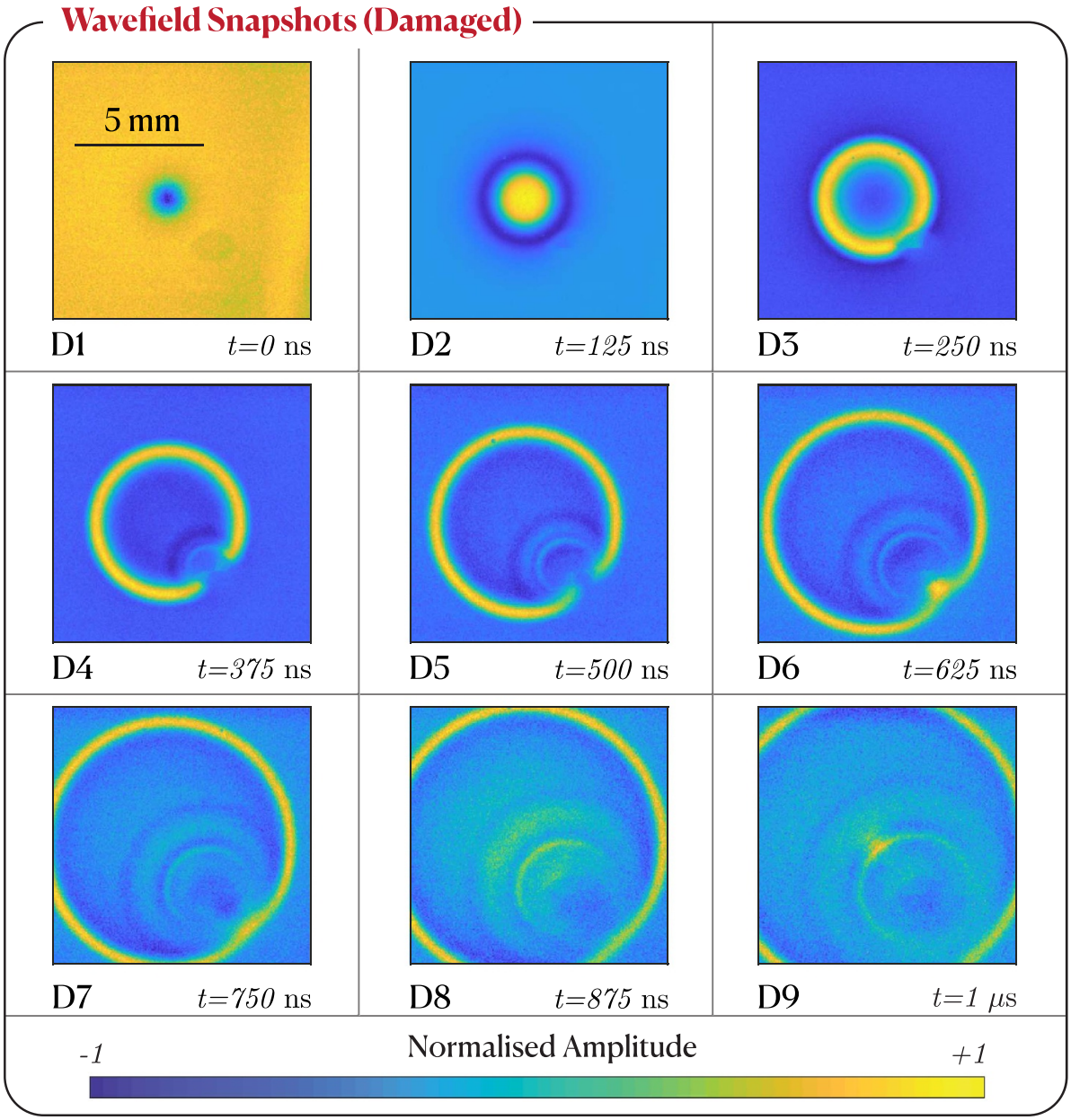

Figure 7. Sequential snapshots of the spatial and temporal evolution of the ultrasonic waves at an interval of 125 ns in a 3 mm thick sintered PZT (damaged state). The dimension of each frame is 10 mm × 10 mm.

figure 6 is 190 ns. The size of the spatiotemporal data matrix is 200 × 200 × 365. The spatial dimension of each snapshot is 200 pixels × 200 pixels, corresponding to the 10 mm × 10 mm in physical space. The total number of 365 such time-varying snapshots are collected by performing an experiment corresponding to the total acquisition time of 1μs. The maximum intensity is observed at the centre of the snapshots H1 and H2 in figure 6 attributed to the strong coupling of the electric field. The circular wave fringe propagating in the outward radial direction is due to the isotropic property of the PZT ceramic.

A controlled surface defect is introduced after completing the Coulomb scanning of the healthy specimen. The damaged specimen is reoriented to minimise the scanning offset with respect to the healthy state, as the scanning is done at different time instances. The sequential snapshots of the spatial and temporal wave propagation in the defected PZT are presented in figure 7. The surface defect acts as a reflector and hinders the propagation of the elastic waves. The forward propagating wave reflects when it encounters the defect boundary and the edges of the specimen. From the snapshots D4–D9 of figure 7 the wave undergoes multiple interferences among the forward-propagating and reflected back-propagating waves.

The precise detection and quantification of anomalies from the sequential wavefield snapshots are challenging, and the multiple interferences among the forward and reflected waves further compound the challenge. Coming to the rescue, a novel algorithm based on a deep autoencoder is manifested to identify the anomaly in the PZT crystal. The main thrust

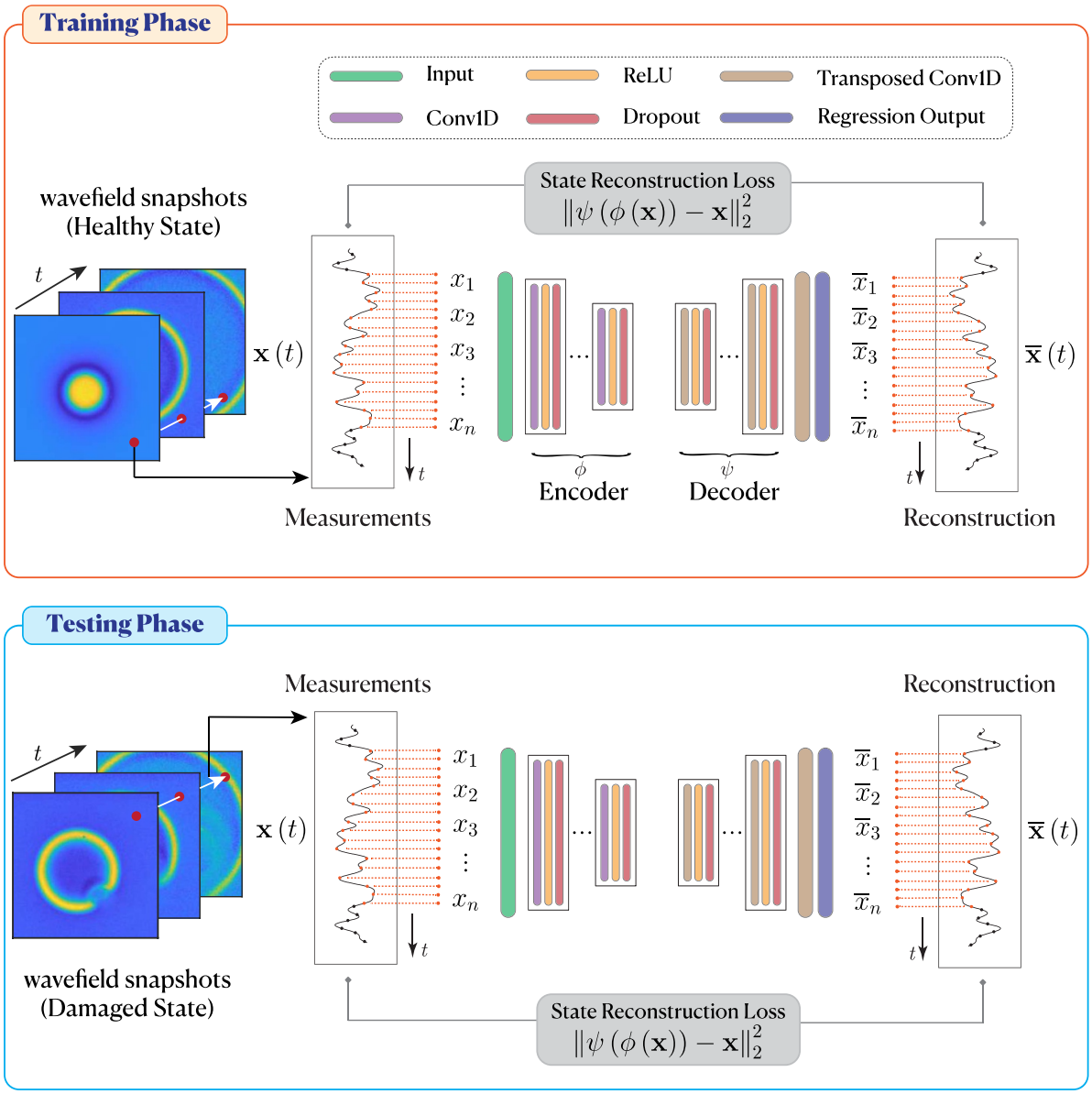

Figure 8. Schematic illustration of the proposed damage detection framework based on deep autoencoder for identifying anomalies in the PZT material.

of this work is to develop a deep learning-based algorithm to detect and localise the damage. The deep autoencoder is ideally suited to extract damage-sensitive features from the complex waveform data. The proposed novel damage detection algorithm has two phases, i.e. (a) damage-sensitive features extraction by employing deep autoencoder, (b) damage localisation by measuring PSNR between the damaged features in the form of images of the healthy and damaged state.

Here, we propose to employ a deep autoencoder to detect anomalous regions in a collection of time series wavefield data. An autoencoder is a type of NN trained to reconstruct the input. This can be achieved by encoding and decoding steps. The encoder transforms the input into a lower dimensional space and reconstruction the input from the lower dimensional space by the decoder. One must note that training an autoencoder does not require labelled data.

The autoencoder itself does not identify anomalies. The basic idea here is training an autoencoder using only a healthy dataset to yield a deep learning model that can reconstruct its input data by using features learned from the trained data only. To detect anomaly in the observed data using an autoencoder, the observed measurement is provided as an input into the trained network, and the error between the input and the reconstructed measurement is evaluated. A significant error between the input and reconstructed measurement indicates that the input measurement consists of features unrepresentative of the data used to train the network; thus, the input measurement is anomalous. By evaluating the region-wise error among the input measurement and reconstructed measurement, one can identify the localised region of defect. The proposed network architecture is illustrated in figure 8. Out of the available healthy time series data in 40 000 $(=200 \times 200)$ spatial

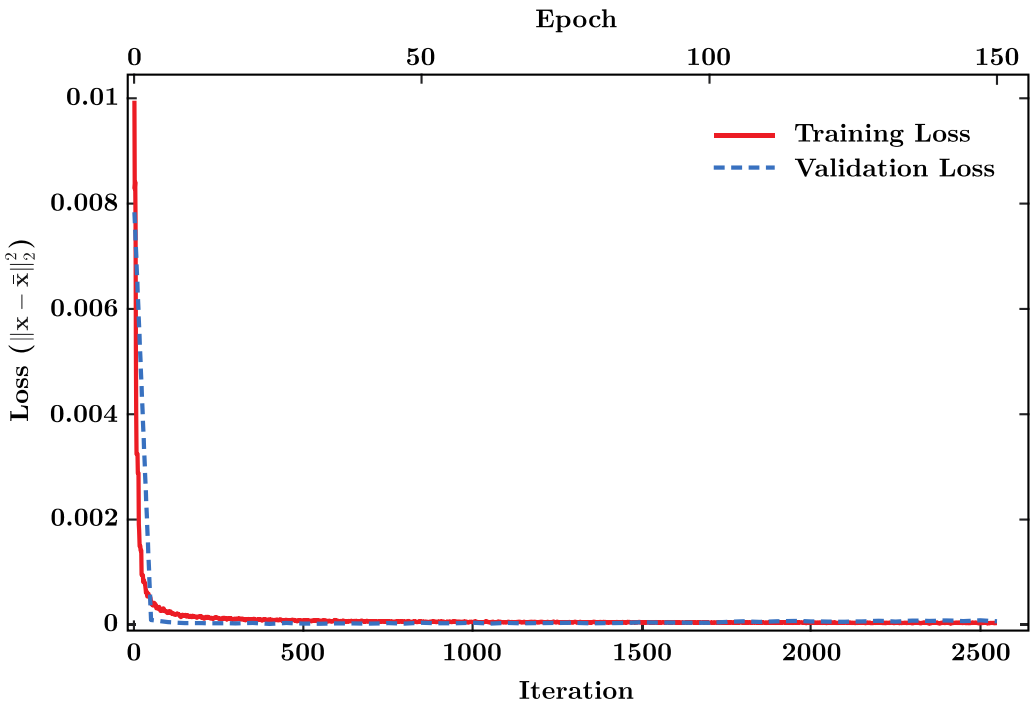

Figure 9. The plot of the performance summary of the optimisation algorithm (red line) during the training and the performance summary of the autoencoder in validation (dashed blue line) during the training process.

locations, the 2500 time series data are selected by uniform sampling to train the autoencoder. The data are partitioned into training and validation partitions. The autoencoder network is trained 90% of the data, and 10% is kept aside for validation.

The encoder of the autoencoder network considered in this work recursively down-samples the temporal dimension of the data by a factor of two. Then, the decoder up-samples the data by a factor of two the same number of times. Before providing the data into the network, the time series data is truncated to have a length of the nearest multiple of 2^j, where j is the number of down-sampling operations to ensure the network can reconstruct the data unmistakably. In this study, $j = 2$ is considered, i.e. the autoencoder network down-samples the data twice.

The input data are normalised using Z-score normalisation to have a better performance in the training process. The encoder network is designed by repeating blocks of 1D convolution, rectified linear unit (ReLU) and dropout layers to down-sample the data. Whereas the decoder is designed by the same number of blocks of 1D transposed convolution, ReLU and dropout layers to up-sample the data, as illustrated in figure 8. The network down-samples and up-samples the data evenly by a factor of 2, specifying the stride equal to 2. Finally, a 1D transposed convolution and regression output layers are included to get the output of the same size as the input. Then, the network is trained with the Adam solver for 17 iterations per epoch. A total number of 2550 iterations corresponding to 150 epochs are required to finish the training process. The validation data are used to validate the network. The variation of training loss and validation loss to the number of iterations and the epochs are illustrated by the red and dashed blue lines, respectively, in figure 9.

After training the deep learning model, the objective is to detect the anomaly in the PZT sensor. Towards that, the MAE between the input sequence and the reconstructed sequence is considered damage sensitive feature. The data collected from the damaged PZT by experimenting are provided as input to the trained deep autoencoder. The MAE is evaluated for each sequence of the damaged PZT data. One must note that the size of the damaged data matrix is $200 \times 200 \times 365$, i.e. 40 000 $(= 200 \times 200)$ number of time sequences are reconstructed by the trained autoencoder network and corresponding MAE are calculated. To compare with the healthy PZT dataset of size $200 \times 200 \times 365$, the similar steps are repeated. Figures 10(a) and (b) illustrate the visualisation of the MAE matrix obtained by applying the deep autoencoder network on healthy and damaged states, respectively.

The deep autoencoder network extracts the damage-sensitive features of the wave interaction with the surface defect. Further, referring to figure 10(b), the MAE image of the damaged state shows the impression of the surface defect. In addition to detecting the defect, the subsequent objective is to quantify and localise the anomaly in the PZT. Towards this objective, the MAE images of the healthy and damaged data are considered. Since the experimental measurement of healthy and damaged data are disjoint and measured independently, it is evident that the 2D wave field images will have geometrical offset and rotation. The MAE images will also possess the offset or rotation as they are extracted from such raw data. A slight offset or rotation can induce a substantial error in anomaly quantification. Intensity-based

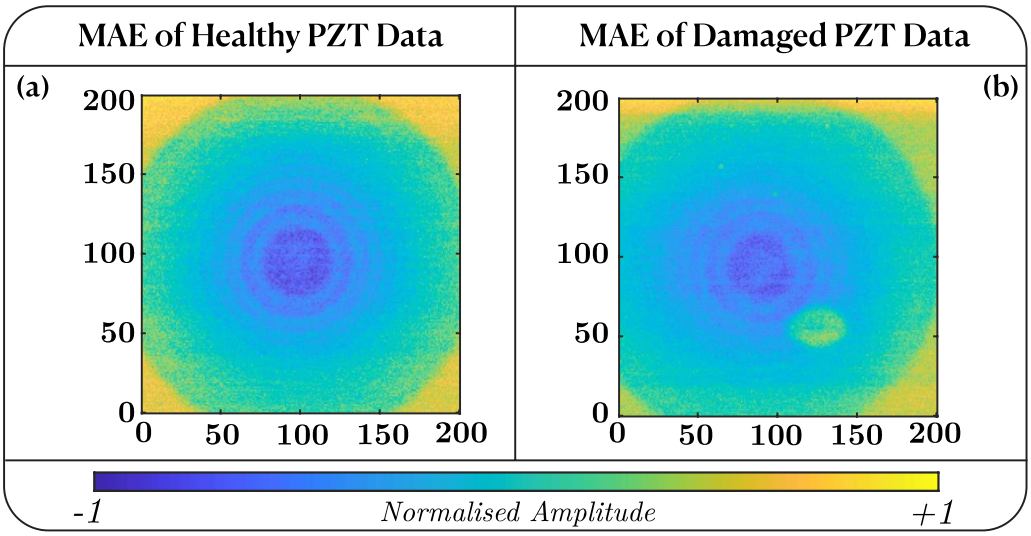

Figure 10. Illustration of the MAE of the autoencoder representation for (a) healthy PZT data and (b) damaged PZT data.

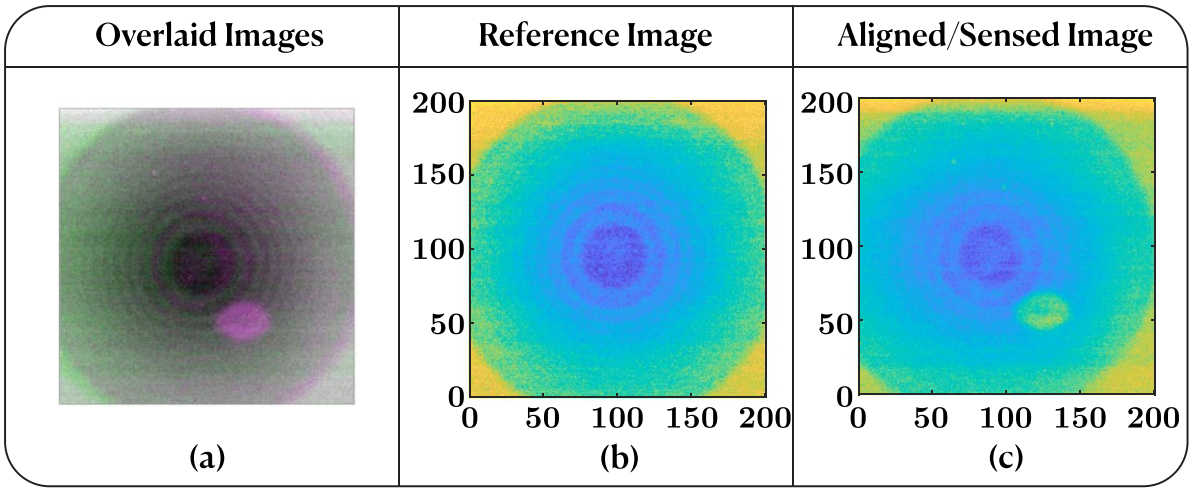

Figure 11. Results of intensity-based image registration. (a) The damaged MAE image (magenta) is overlaid on the healthy MAE image (green), (b) the aligned reference image, and (c) the aligned MAE image of damaged data.

image registration is employed to address the challenge arising due to offset. From figure 11(a), it can be observed that the MAE image of the damaged data is considered a sensed image (magenta) and the MAE image of healthy data as a reference image (green) in the intensity-based image registration. The result of the offset correction is illustrated in figure 11.

After the registration process is performed, the quantification and localisation of the surface anomaly are done by computing PSNR values. The key idea of evaluating the PSNR value is computing the difference between healthy and damaged MAE images. The MAE image of the damaged state almost exhibits the MAE image of the healthy state with the loss of some information at the damaged location. The MAE images are divided into 400 grids, and the dimension of each grid is $10\,pixels \times 10\,pixels$ $(0.5\text{ mm} \times 0.5\text{ mm})$ as shown in figure 12(b). The PSNR is computed between the healthy and damaged MAE images on each grid. As discussed in section 5, the PSNR value will be maximum for similar grids. The computation of PSNR values in dB by considering the grids is illustrated in figure 12(a).

Referring to figure 12(a), the PSNR values suddenly abate for the grid numbers 235, 254, 255, 256, 274 and 275. These grids are identified on the MAE image of the damaged state, which conforms to the location of the defect, as illustrated in figure 12(c). The size of these anomalous six grids is quantified as $1.5\text{ mm}^2\,(=6\times 0.5\text{ mm}\times 0.5\text{ mm})$. The original size of the surface defect is approximately $1.56\text{ mm}^2\,(=1.2\text{ mm}\times 1.3\text{ mm})$. Therefore, the proposed algorithm is accurate for the detection, localisation and quantification of the surface anomaly on PZT sensors with an accuracy of about 96%.

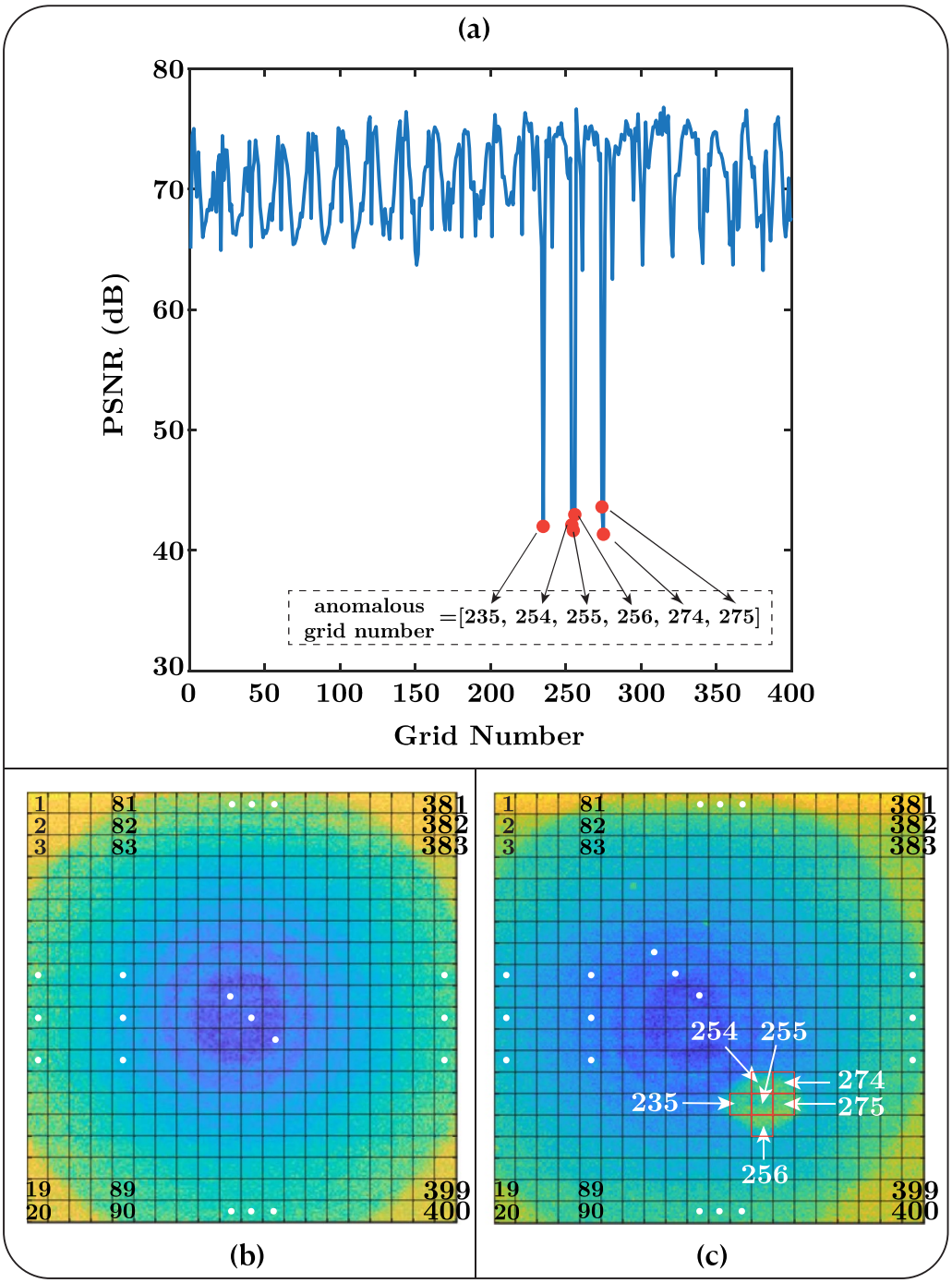

Figure 12. (a) The plot of PSNR values in dB to the grid number, (b) an illustration of the grids used on the MAE image of the healthy state, and (c) identification of anomalous grids on the MAE image of the damaged state.

7. Conclusion

The autoencoder NN is a data-driven deep learning technique that learns the crucial features from healthy data. The unique learning ability of the autoencoder NN is leveraged to extract the damage-sensitive features from the data. The novel experimental technique based on Coulomb coupling is employed to visualise the spatial–temporal evolution of the ultrasonic waves in the PZT sensor. The received sequential temporal signals of the excited ultrasonic wave in the PZT are considered for detecting and quantifying the surface defect in the PZT. The autoencoder provides an input–output deep learning model for the interaction of waves with complex geometries. The MAE between the input signal and reconstructed signal by the autoencoder NN is sensitive to defect and is considered for quantification and localisation. Further, PSNR is computed between the MAE images of healthy and damaged datasets to localise the anomaly. The proposed robust algorithm manifests good accuracy in detecting and quantifying the anomaly with an accuracy of about 96%. Albeit, the

proposed framework being implemented on full-field transient signals of healthy and damaged states has still poised itself to perform satisfactorily in situations of data sparsity and without healthy state data that needs further investigation.

Data availability statement

All data that support the findings of this study are included within the article (and any supplementary files).

Acknowledgments

Amit Shelke and Nur M M Kalimullah would like to acknowledge Indian Space Research Organisation (ISRO) for supporting this work under Grant Number ISRO/RES/STC/IITG/2021-22. A Habib acknowledges Cristin Project, Norway, ID: 2061348 (Habib) for supporting this work.

ORCID iDs

Nur M M Kalimullah https://orcid.org/0000-0003-0447-6527
Amit Shelke https://orcid.org/0000-0001-5662-1453
Anowarul Habib https://orcid.org/0000-0001-6515-3145

References

[1] Bhalla S and Soh C K 2004 Structural health monitoring by piezo-impedance transducers. I: modeling *J. Aerospace Eng.* **17** 154–65
[2] Providakis C P, Stefanaki K D, Voutetaki M E, Tsompanakis Y and Stavroulaki M 2014 Damage detection in concrete structures using a simultaneously activated multi-mode PZT active sensing system: numerical modelling *Struct. Infrastruct. Eng.* **10** 1451–68
[3] Hwang G T, Annapureddy V, Han J H, Joe D J, Baek C, Park D Y, Kim D H, Park J H, Jeong C K and Park K I 2016 Self-powered wireless sensor node enabled by an aerosol-deposited PZT flexible energy harvester *Adv. Energy Mater.* **6** 1600237
[4] Shelke A, Kundu T, Amjad U, Hahn K and Grill W 2011 Mode-selective excitation and detection of ultrasonic guided waves for delamination detection in laminated aluminum plates *IEEE Trans. Ultrason. Ferroelectr. Freq. Control* **58** 567–77
[5] Shung K K 2015 *Diagnostic Ultrasound: Imaging and Blood Flow Measurements* 2nd Edn (CRC Press) (https://doi.org/10.1201/b18323)
[6] Farrar C R and Lieven N A 2007 Damage prognosis: the future of structural health monitoring *Phil. Trans. R. Soc.* A **365** 623–32
[7] Hui L and Jinping O 2011 Structural health monitoring: from sensing technology stepping to health diagnosis *Proc. Eng.* **14** 753–60
[8] Jata K V, Kundu T and Parthasarathy T A 2010 An introduction to failure mechanisms and ultrasonic inspection *Advanced Ultrasonic Methods for Material and Structure Inspection* (Wiley-ISTE) pp 1–42
[9] Djurdjanovic D, Ni J and Lee J 2002 Time-frequency based sensor fusion in the assessment and monitoring of machine performance degradation, *ASME Int. Mechanical Engineering Congress and Exposition* vol 36290
[10] Brownjohn J M 2007 Structural health monitoring of civil infrastructure *Phil. Trans. R. Soc.* A **365** 589–622
[11] Farrar C R, Worden K, Lieven N A and Park G 2010 Nondestructive evaluation of structures *Encyclopedia of Aerospace Engineering* (Wiley) (https://doi.org/10.1002/9780470686652.eae186)
[12] Todd M, Nichols J, Pecora L and Virgin L 2001 Vibration-based damage assessment utilizing state space geometry changes: local attractor variance ratio *Smart Mater. Struct.* **10** 1000–8
[13] Quek S, Tua P and Jin J 2007 Comparison of plain piezoceramics and inter-digital transducer for crack detection in plates *J. Intell. Mater. Syst. Struct.* **18** 949–61
[14] Duncan M D, Bashkansky M and Reintjes J 1998 Subsurface defect detection in materials using optical coherence tomography *Opt. Express* **2** 540
[15] Rose J L and Nagy P B 2000 Ultrasonic waves in solid media *J. Acoust. Soc. Am.* **107** 1807–8
[16] Kundu T 2003 *Ultrasonic Nondestructive Evaluation: Engineering and Biological Material Characterization* (CRC Press) (https://doi.org/10.1201/9780203501962)
[17] Kundu T, Di Scalea F L and Sohn H 2016 Structural health monitoring: use of guided waves and/or nonlinear acoustic techniques *Opt. Eng.* **11001** 1
[18] Pamwani L, Habib A, Melandsø F, Ahluwalia B S and Shelke A 2018 Single-input and multiple-output surface acoustic wave sensing for damage quantification in piezoelectric sensors *Sensors* **18** 2017
[19] Kalimullah N M M, Shelke A and Habib A 2021 Multiresolution dynamic mode decomposition (mrDMD) of elastic waves for damage localisation in piezoelectric ceramic *IEEE Access* **9** 120512–24
[20] Habib A, Shelke A, Pluta M, Kundu T, Pietsch U and Grill W 2012 Imaging of acoustic waves in piezoelectric ceramics by coulomb coupling *Jpn. J. Appl. Phys.* **51** 07GB05
[21] Shelke A, Habib A, Amjad U, Pluta M, Kundu T, Pietsch U and Grill W 2011 Metamorphosis of bulk waves to Lamb waves in anisotropic piezoelectric crystals *Health Monit. Struct. Biol. Syst.* **7984** 341–52
[22] Kalimullah N M M, Shukla K, Shelke A and Habib A 2023 Stiffness tensor estimation of anisotropic crystal using point contact method and unscented Kalman filter *Ultrasonics* **131** 106939
[23] Agarwal V, Shelke A, Ahluwalia B, Melandsø F, Kundu T and Habib A 2020 Damage localization in piezo-ceramic using ultrasonic waves excited by dual point contact excitation and detection scheme *Ultrasonics* **108** 106113
[24] Habib A, Shelke A, Pluta M, Pietsch U, Kundu T and Grill W 2012 Scattering and attenuation of surface acoustic waves and surface skimming longitudinal polarized bulk waves imaged by Coulomb coupling *AIP Conf. Proc.* **1433** 247–50
[25] Habib A, Twerdowski E, von Buttlar M, Wannemacher R and Grill W 2007 The influence of the radius of the electrodes employed in Coulomb excitation of acoustic waves in piezoelectric materials *Health Monit. Struct. Biol. Syst.* **6532** 381–9
[26] Yu M H and Kim H S 2021 Deep-learning based damage sensing of carbon fiber/polypropylene composite via addressable conducting network *Compos. Struct.* **267** 113871
[27] Babajanian Bisheh H, Ghodrati Amiri G, Nekooei M and Darvishan E 2019 Damage detection of a cable-stayed bridge using feature extraction and selection methods *Struct. Infrastruct. Eng.* **15** 1165–77
[28] Isranuri I 2020 Bearing damage detection using support vector machine *IOP Conf. Ser.: Mater. Sci. Eng.* **851** 012063
[29] Schmidt S, Zimroz R and Heyns P S 2021 Enhancing gearbox vibration signals under time-varying operating conditions

by combining a whitening procedure and a synchronous processing method *Mech. Syst. Signal Process.* **156** 107668
[30] Jia F, Lei Y, Lin J, Zhou X and Lu N 2016 Deep neural networks: a promising tool for fault characteristic mining and intelligent diagnosis of rotating machinery with massive data *Mech. Syst. Signal Process.* **72** 303–15
[31] Schmidhuber J 2015 Deep learning in neural networks: an overview *Neural Netw.* **61** 85–117
[32] Bengio Y, Courville A and Vincent P 2013 Representation learning: a review and new perspectives *IEEE Trans. Pattern Anal. Mach. Intell.* **35** 1798–828
[33] Shang C, Yang F, Huang D and Lyu W 2014 Data-driven soft sensor development based on deep learning technique *J. Process Control* **24** 223–33
[34] Bort W, Baskin I I, Gimadiev T, Mukanov A, Nugmanov R, Sidorov P, Marcou G, Horvath D, Klimchuk O and Madzhidov T 2021 Discovery of novel chemical reactions by deep generative recurrent neural network *Sci. Rep.* **11** 3178
[35] Hendriksen A A, Bührer M, Leone L, Merlini M, Vigano N, Pelt D M, Marone F, Di Michiel M and Batenburg K J 2021 Deep denoising for multi-dimensional synchrotron x-ray tomography without high-quality reference data *Sci. Rep.* **11** 11895
[36] Sagheer A and Kotb M 2019 Unsupervised pre-training of a deep LSTM-based stacked autoencoder for multivariate time series forecasting problems *Sci. Rep.* **9**
[37] Peng C, Chen Y, Gui W, Tang Z and Li C 2022 Remaining useful life prognosis of turbofan engines based on deep feature extraction and fusion *Sci. Rep.* **12** 6491
[38] Fukushima K, Miyake S and Ito T 1983 Neocognitron: a neural network model for a mechanism of visual pattern recognition *IEEE Trans. Syst. Man Cybern.* **SMC-13** 826–34
[39] Cybenko G 1992 Approximation by superpositions of a sigmoidal function *Math. Control. Signals Syst.* **5** 455
[40] Hornik K, Stinchcombe M and White H 1989 Multilayer feedforward networks are universal approximators *Neural Netw.* **2** 359–66
[41] Hornik K, Stinchcombe M and White H 1990 Universal approximation of an unknown mapping and its derivatives using multilayer feedforward networks *Neural Netw.* **3** 551–60
[42] LeCun Y, Bengio Y and Hinton G 2015 Deep learning *Nature* **521** 7553
[43] Goodfellow I, Bengio Y and Courville A 2016 *Deep Learning* (MIT Press)
[44] Lin Y Z, Nie Z H and Ma H W 2017 Structural damage detection with automatic feature-extraction through deep learning *Comput. -Aided Civ. Infrastruct.* **32** 1025–46
[45] Liu Z, Cao Y, Wang Y and Wang W 2019 Computer vision-based concrete crack detection using U-net fully convolutional networks *Autom. Constr.* **104** 129–39
[46] Shao H, Jiang H, Zhao H and Wang F 2017 A novel deep autoencoder feature learning method for rotating machinery fault diagnosis *Mech. Syst. Signal Process.* **95** 187–204
[47] Kalimullah N M M, Shelke A and Habib A 2023 A probabilistic framework for source localization in anisotropic composite using transfer learning based multi-fidelity physics informed neural network (mfPINN) *Mech. Syst. Signal Process.* **197** 110360
[48] Khan A, Ko D-K, Lim S C and Kim H S 2019 Structural vibration-based classification and prediction of delamination in smart composite laminates using deep learning neural network *Composites* B **161** 586–94
[49] Bang H-T, Park S and Jeon H 2020 Defect identification in composite materials via thermography and deep learning techniques *Compos. Struct.* **246** 112405
[50] Mardanshahi A, Nasir V, Kazemirad S and Shokrieh M 2020 Detection and classification of matrix cracking in laminated composites using guided wave propagation and artificial neural networks *Compos. Struct.* **246** 112403
[51] Qian C, Ran Y, He J, Ren Y, Sun B, Zhang W and Wang R 2020 Application of artificial neural networks for quantitative damage detection in unidirectional composite structures based on Lamb waves *Adv. Mech. Eng.* **12** 168781402091473
[52] Rautela M and Gopalakrishnan S 2021 Ultrasonic guided wave based structural damage detection and localization using model assisted convolutional and recurrent neural networks *Expert Syst. Appl.* **167** 114189
[53] Melville J, Alguri K S, Deemer C and Harley J B 2018 Structural damage detection using deep learning of ultrasonic guided waves *AIP Conf. Proc.* **1949** 230004
[54] Zitova B and Flusser J 2003 Image registration methods: a survey *Image Vis. Comput.* **21** 977–1000
[55] Hore A and Ziou D 2010 Image quality metrics: PSNR vs. SSIM *20th Int. Conf. on Pattern Recognition* (https://doi.org/10.1109/ICPR.2010.579)
[56] Habib A, Shelke A, Pietsch U, Kundu T and Grill W 2012 Determination of the transport properties of ultrasonic waves traveling in piezoelectric crystals by imaging with Coulomb coupling *Health Monit. Struct. Biol. Syst.* **8348** 316–24
[57] Habib A, Twerdowski E, von Buttlar M, Pluta M, Schmachtl M, Wannemacher R and Grill W 2006 Acoustic holography of piezoelectric materials by Coulomb excitation *Health Monitoring and Smart Nondestructive Evaluation of Structural and Biological Systems V* vol 6177
[58] Brunton S L and Kutz J N 2022 *Data-driven Science and Engineering: Machine Learning, Dynamical Systems, and Control* (Cambridge University Press)
[59] Gin C R, Shea D E, Brunton S L and Kutz J N 2021 DeepGreen: deep learning of Green's functions for nonlinear boundary value problems *Sci. Rep.* **11** 21614
[60] Brown L G 1992 A survey of image registration techniques *ACM Comput. Surv.* **24** 325–76